Proceedings of ASME Turbo Expo 2011
GT2011
June 6-10, 2011, Vancouver, British Columbia, Canada

GT2011-45267

COMPUTATIONAL STUDY OF MICRO-JET IMPINGEMENT HEAT TRANSFER IN A HIGH PRESSURE TURBINE VANE

Karan Anand **B. A. Jubran**

Department of Aerospace Engineering
Aero-Thermal Management Laboratory
Ryerson University, 350 Victoria St., Toronto, ON, M5B 2K3, Canada

ABSTRACT

The purpose of this numerical investigation is to study the micro-jet impingement heat transfer characteristics and hydromechanics in a 3-D, actual-shaped turbine vane geometry. No concession is made on either the skewness or curvature profile of the airfoil in the streamwise direction, nor to the lean, airfoil twist or tapering of the vane in the spanwise direction. The problem on hand consists of a constant property flow of air via an array of 42 round micro jets impinging onto the inner surface of the airfoil. For simplicity, validation and better understanding of the nature of impingement heat transfer, the airfoil surfaces are provided with a constant temperature boundary condition. Validation is performed against existing numerical results on a simplified model with no spanwise tapering or twisting. The modeled volume spans a total of 12D and consists of three rows of jets; each row contains 14 inline jets. Governing equations are solved using a finite volume method in FLUENT. Effects of jet inclination (+45° and -45° inclinations) and decrease in nozzle diameter (0.51, 0.25 and 0.125 mm) are studied. Inclination of -45° produced enhanced mixing and secondary peaks with marginal decrease in stagnation values. The effect of reducing the diameter of the jets yielded positive results; the tapering effect too enhanced the local heat transfer values, which is attributed to the increase in local velocities at jet exit.

INTRODUCTION

Cooling systems for hot flow path components in a modern gas turbine engine are required to outperform with regards to the cooling effectiveness and efficiency. To meet the desired metal temperature with high thermodynamic efficiency it is preferred to achieve low coolant-flow rates and reduced mixing losses when coolant is returned to the flow path [1]. Jet impingement cooling has a substantial potential to achieve high local heat transfer coefficients while maintaining globally, low coolant-flow rates [2]. Although various cooling schemes such as film cooling, convective and impingement cooling with turbulence promoters and pin-fins are employed in the first stage of turbine vanes, the current study pertains to parametric analysis of micro-jet impingement in a high pressure vane. Hence, the model chosen is a second staged NASA-GE Energy Efficient Engine (E^3) vane where the primary cooling method is convection cooling by a single impingement insert [1]. The coolant air enters the impingement insert in the spanwise direction, impinges perpendicularly on the inner airfoil surface, and exits at the trailing edge, effectively cooling the vane. The bleed air is fed from the seventh staged compressor stator to the turbine vanes. Array of jets are thus used to reduce the excessive localized heat loads on the vane thereby increasing its life and cooling efficiently.

Array of jets perform differently from a single jet; the main contributor being the cross-flow developed from upstream spent jets. Koopman and Sparrow [3] showed the effect of cross-flow on the array of inline jets and compared the results to single radial jet. It was shown that the oncoming flow rate altered the performance of neighboring jets. The experimental work of Florschuetz et al. [4] assessed different parameters which affect the cross-flow distribution across the array; a cross-flow to jet mass flow velocity ratio was derived in this model and was seen to be independent of the streamwise spacing of the array. However, the ratio was a function of jet to target spacing and the spanwise spacing; the cross-flow experienced by the jets decreases with an increase in any of these functional parameters. The hydrodynamics of impinging flow from array of nozzles is quite similar to a single jet impingement and shows similar flow regimes: free jet, stagnation zone, wall jet and recirculation zone in case of confinement. In addition, secondary stagnation zones may be seen due smaller spacing between jets. This zone is characterized by boundary layer separation and eddying of flow

[5]. The heat transfer under an impinging array is typically resolved in the streamwise direction. Key parameters which influence the heat transfer rate are: the nozzle geometry, Reynolds number (Re), the cross-flow ratio, the streamwise and spanwise spacing, the jet to target spacing, angle of impact and the exit/entrance conditions [6]. Mentioned in Martin's [5] paper is the result obtained by Korger and Krizek in relation to the inclination of jets; the stagnation point was shifted by a length ΔX towards the part of the jet that creates acute angle. Huang et al. [7] performed experimental work in studying inclined jets and found that inclined jets under perform with respect to heat transfer coefficients than straight jets; the supporting argument for reduction in cooling being that cross-flow tends to diffuse the impingement effect. Similar studies [2,7] were performed to see the effect of cross-flow direction on heat transfer where the exit conditions were changed. The cross-flow shifted the jet impingement location and reduced the stagnation and local Nusselt number (Nu).

Experimental work in gas turbine engine usually models the vane as a flat plate. References [4,8-10] are instances of such work for gas turbine application. Also, most experimental work such as above, penetrate the flow into the nozzle not in normal direction but parallel directions. That is, the inlets are aligned in the direction of jet discharge. The current study, however, uses true 3D vane profiles with flow entering the plenum in the spanwise direction and flow impinging orthonormal to this direction. To the best of authors' knowledge, it seems to-date that, most of the work on jet impingement cooling for turbine application is limited to flat plate impingement and leading edge and that there is no or limited reported study in the open literature on numerical analysis of fully defined 3D turbine vane model with micro jets. This paper uses 3D turbine vane spanning length of 12D in the radial direction with true airfoil profiles. Validation is performed against existing numerical results on a simplified model with no spanwise tapering or twisting. The model considered not only changes the inclination of the jets but also the diameter of the nozzle jets. Experimental work and flow predictions in case of inclined jet impingement on flat plate are presented above. For the case of reducing the jet diameter, experimental analysis was performed by Lee and Lee [11] with micro sized (0.25 mm) nozzle diameter. This analysis was performed with single jet impingement and not array of jets. The effect of diameter on the local Nu was negligibly small for wall jet region due to impinging flow effects being diminished for r/D>0.5 (r being the radial direction on the target plate). However, the stagnation Nu values were seen to increase by about 30%. This value was obtained for a large jet to target distance. In an experimental setup by Glynn and Murray [12], about 20% to 70% increase was seen in stagnation values when jet diameter was reduced to 1 mm from 1.5 mm. This case also pertains to flat plate with single jet, but with confinement (as shown in Figure 1) added as opposed to the former case.

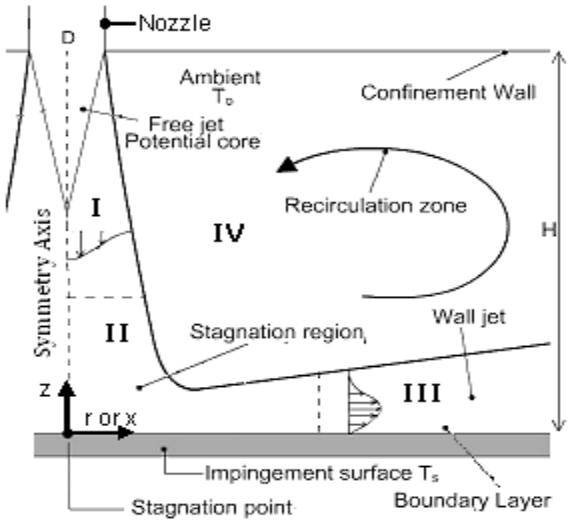

Figure 1: Single Jet Impingement Flow Physics (Modified From Original) [6]

Model Considerations

Due to the small diameter of jets, there is an increased probability that the system may deviate from the established no slip condition or continuum laws. Using the plenum pressure, P, for air at 500 K (see validation vane below for boundary and operating conditions) and the equation of state, the mean free path (λ) for air was calculated using equation (1), where d is the diameter of air molecule and N_A is the Avogadro's number.

$$\lambda = \frac{RT}{\sqrt{2}\pi d^2 N_A P} \tag{1}$$

The Knudsen number (K_n; see equation (2)) for jet diameter of 0.125 mm (smallest selected) are in order of ($10^{-5} \approx 0$) at P of ~1.4 MPa. $0 < K_n < 0.1$ is referred to as slip flow [13]; no-slip is captured by $K_n = 0$ [14]. Hence, the laws are valid and consequently, the regular Navier-Stokes equation has been used for solving the problem.

$$K_n = \frac{\lambda}{D} \tag{2}$$

For evaluation of heat transfer between the fluid and target plate, the convective heat transfer coefficient, h, is defined. Also, the dimensionless Nu, is introduced to measure the cooling effect due to impingement in equation (3). Here, q_s is the surface heat flux and L_c is the characteristic length chosen to be the chord length of the airfoil.

$$h = \frac{q_s}{T_s - T_j} \qquad Nu = \frac{hL_c}{k} \tag{3}$$

Another consideration or rather concern for small diameter jets is the fact that small jets tend to be expensive to manufacture (for instance, using electro stream process or laser beam machining) and may be prone to plugging/blockage

[1,15]. Various patents have been filed and numerous researches are being performed to protect such blockages, see references [16] [17] as examples. All recommendations suggested geometric changes around the inlet to the plenum and cooling passages leading to the insert. This paper assess micro jet cooling assuming there is no blockage and that substantial parallel research is being performed to achieve this goal.

MODEL GEOMETRY

The modeled second-staged high-pressure turbine vane is part of the E^3, whose studies were conducted by the General Electric Company for NASA. Airfoil coordinates are provided in a report by Timko [18]. Two models were generated, one for validation and other as the base model. The base model was then used for parametric analysis. The vane consists of a single plenum chamber defined by the impingement insert and the design utilizes convection only cooling, making it an excellent choice for the study of impingement cooling in a real vane. The flow considered is incompressible; steady state solution is obtained for flow of air at 500 K impinging on the airfoil surfaces. The holes are 0.51 mm in diameter and an array of 42 jets are studied. The modeled volume spans a total of 12D and consists of three columns of jets; each contains 14 rows of jets: one for leading edge, seven for the pressure surface and remaining for the suction surface cooling. The spanwise spacing between holes was kept at 4D for the base model.

Figure 2 depicts the geometric problem under consideration. The model shown is the fluid domain control volume. Air enters in the –Z direction into the plenum chamber, making the blue surface (below) as the inlet boundary. Flow thus moves in the spanwise direction; due to the pressure difference between the two chambers (plenum chamber, shown in blue and impingement chamber, shown in pink in Figure 2), air impinges on the airfoil surface via the nozzles colored in green. The purple arrow shows the direction of the flow from the inlet face. The orange arrow shows the outlet flow. The red arrows show the spanwise and streamwise directions. The arrows within the impingement chamber (pink) show the streamwise cross-flow direction and lastly, the arrows within the plenum chamber (blue) show the impingement flow direction. The other end of the plenum chamber that is opposite to the inlet flow is closed. Also, the jet flow passage is closed on both sides by walls. The arrows show the direction of flow only. After impinging the airfoil surface, the flow is forced to exit at the outlet boundary at the trailing edge of the vane in the streamwise direction. Since all the flow entering the inlet has to exit the outlet to conserve mass, the jet flow consumes flow in its entirety. Figure 3 illustrates the flow in the section with transparency. Parameters like nozzle length, L, and jet to target spacing, H, are also defined in the figure.

The parametric values chosen for the base model, tested parameters and other geometric reference values used for obtaining the results are provided in Table 1 below. The values chosen for span, jet Spacing, L and H are for validation purposes and the values closely mimic true values. The characteristic reference value used is the chord length. Although this length changes locally, the mid span chord length was used as a reference value. Also, this was the reference value used by Leon De Paz [6]; and, the current vane is validated against the same work by Leon De Paz [6]. The difference between the base model and validation model is shown in Figure 4 (e) and (d) respectively. The Base model is part of the midsection of the actual vane profile presented in Figure 4 (a). The airfoil sections at the different span locations are also shown for clarity (Figure 4 (b)). The effect of tapering, skewedness and twisting are clearly noticed when they are overlapped in Figure 4 (c). In Figure 4, the purple arrows show the direction of the flow from the inlet face and the orange arrows show the outlet flow at the trailing edge. Note that the other end of plenum chamber opposite to the inlet flow is closed (marked as 'wall' in Figure 4 (a) and (b).

The models for inclined jets are displayed in Figure 5. The convention defined for the inclination of jets is: positive inclination of jets is when the nozzles are aligned in the direction of the streamwise cross-flow buildup from the leading edge. Also, the jets are angled such that the symmetric axis of the inclined nozzle matches the target surface at the same point where the symmetric axis of the base model did. This would allow for easier comparison between the models. The difference

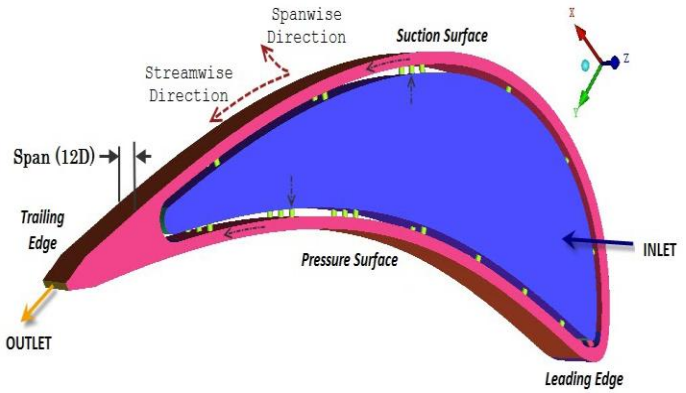

Figure 2: Base Model Geometrical Configuration

Table 1: Parametric and Reference Values for the Geometry

Span/D	12
L/D	1.05
H/D	1.588
Jet spacing/D	4
D[1]	0.51, 0.25 and 0.125 mm
Nozzle Inclination[2]	90°, +45° and -45°
True Vane span	68.326 mm
Reference Chord Length, L_c	66 mm

[1] Parameters such as the span, jet spacing, L and H are non-dimensionalized using nozzle diameter of 0.51 mm. These ratios do not change when diameter is varied for testing. See the results section below for reasoning.

[2] Inclination angles provided are at nozzle diameter of 0.51 mm

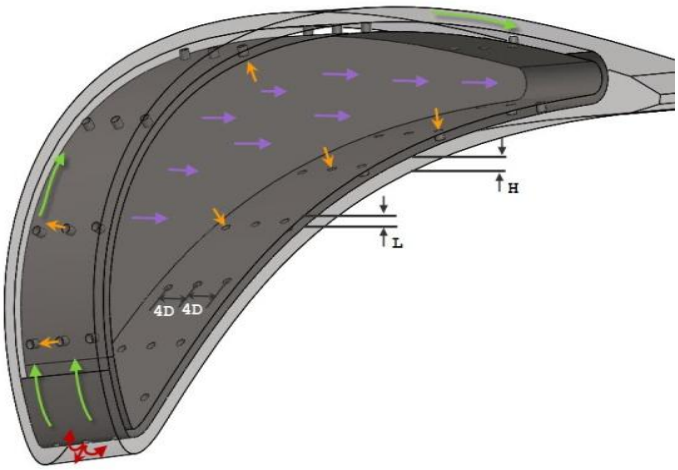

Figure 3: Base Model showing Geometric Parameters and Flow Directions

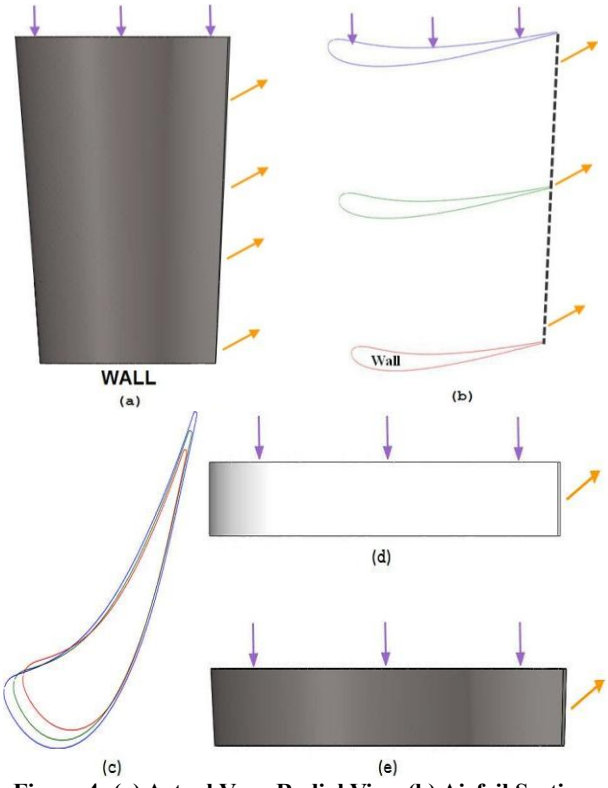

Figure 4: (a) Actual Vane Radial View (b) Airfoil Sections corresponding to figure 4a (c) Airfoil Sections Overlapped (d) Validation Model (e) Base Model

in micro jets are not put on view as the only difference is that the jets are smaller in diameter.

For simplicity, validation and better understanding the nature of impingement heat transfer, the airfoil surfaces (target) are provided with a constant temperature boundary condition. All other walls are kept adiabatic. The airfoil temperature is maintained at 300 K and the impinging fluid is maintained at 500 K. This was mainly done for validation purposes; also, various experimental testing for the same application is performed in this manner; besides, the aim of the paper is to show the effects of heat transfer coefficients, which is independent of the temperature[3]. An added benefit for using such a boundary condition is that the solution convergence issue is avoided [19]. The inlet boundary condition is provided as velocity inlet and is given an inlet velocity of 1.2266 m/s to achieve constant mass flow of 0.003269 kg/s. Fluid properties where changed too; density was changed to behave as incompressible ideal gas due high absolute pressures in the plenum. Constant air properties at 500 K were used otherwise: viscosity at 2.6375×10^{-5} kg/ms, thermal conductivity at 0.040284 W/mK and specific heat value at 1030.305 J/kgK [6, 18]. Furthermore, it was assumed that the flow in its entirety exits from the trailing edge and no leakages occur (especially at inter-stage seal).

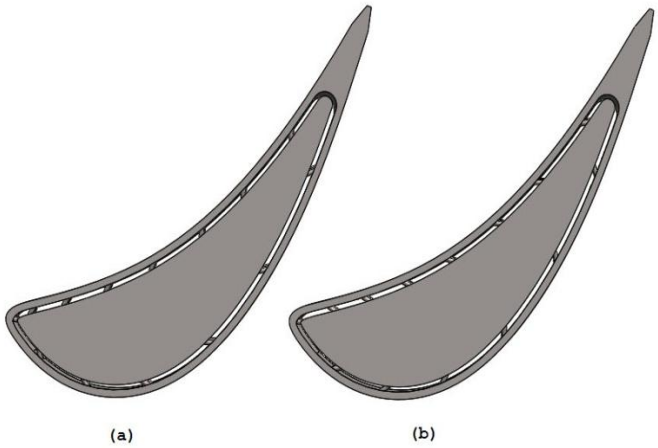

Figure 5: Inclined Jets at D=0.51 mm (a) +45° (b) -45°

Meshing and CFD Simulation Setup

The control volume above was modeled in SolidWorks and the meshing was performed in ICEM-CFD (the mesh structure is shown in Figure 6); the fluid domain was filled with a conformal unstructured hybrid mesh; that is, tetrahedral mesh structure on all surfaces and volumes with hex-core and prism boundary layer. The volumes were split into three with plenum acting as reservoir, the jets and the impingement region. The jet inlet and outlet surfaces were provided as interior surface for the flow to pass through. Different mesh densities were used based on importance of the location. Boundary layer mesh was maintained at target surfaces only as shown below in Figure 7. The plenum mesh was made hybrid to reduce on time taken for solving. The hex-core cut down the mesh by roughly 60%. A cut plane through the model is revealed in Figure 8 showing the hybrid mesh.

[3] Calculations shows that no slip condition is valid for D = 0.125 mm in both cases, here and in true conditions of vane cooling.

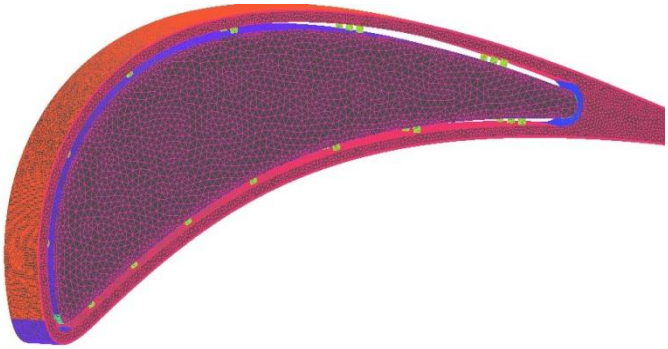

Figure 6: Mesh Structure for Base Model

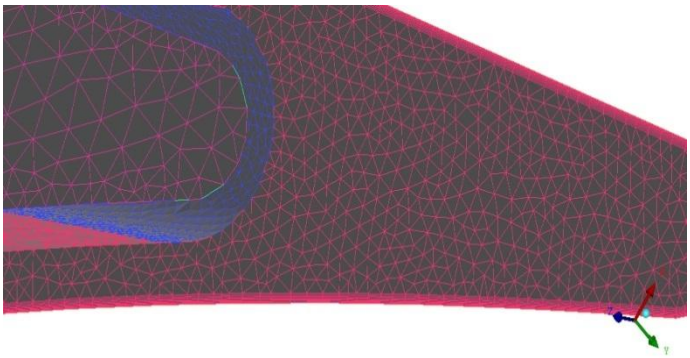

Figure 7: Boundary Layer Mesh with Surface Mesh

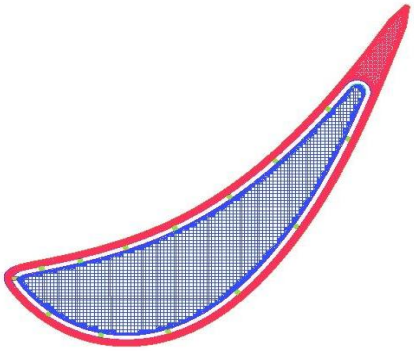

Figure 8: Hybrid Mesh Structure (Cut Plane View)

The mesh structure remained the same for all tests. The mesh size was changed appropriately confirming mesh independence for all cases tested. The mesh size was approximately 355,000 for the intermediate case with D = 0.51 mm. The average Y^+ was maintained below 1 and the max recorded Y^+ was 4.83 near the trailing edge. The maximum y^+ value was kept within 5 enabling the use of enhanced wall functions for the mainly turbulent boundary layer at impingement region and allowing blending functions for regions with higher Y^+ value; for instance, the max recorded Y^+. For a reasonable representation of velocity profiles, it was suggested to maintain y^+ within five [19,20].

CFD simulation was conducted in Fluent. The boundary conditions have been mentioned previously. Implicit, segregated based solver was used with pressure-velocity coupling set to SIMPLE algorithm. The relaxation parameters were tweaked accordingly for maintaining stability or achieving faster convergence. Spatial accuracy of the solution was improved by using second order upwind scheme. Convergence was defined when parameters such as velocity, pressure and temperature were non responsive to many iterations at surface monitors. The monitored surfaces were the inlet and outlet of jets, vane outlet and target airfoil surfaces. All cases showed that the residuals obtained were well below 10^{-5}.

Various studies have been dedicated to modeling turbulence; selecting a turbulence model greatly determines how accurate the solution to the problem can be predicted. A review of impingement heat transfer and turbulence modeling is described by Zuckerman and Lior [21]. It was found that for k-ε model, excessive kinetic energy prediction at stagnation region was a disadvantage. Similar over-prediction (about 300% at stagnation) was seen by Ashforth-Frost and Jambunathan [22] for the same turbulence model, however, for single jets. The best turbulence model, apart from DNS/LES, was the v^2-f model [23]; but, this accuracy was achieved at a higher computational cost. For the case of impingement with application to gas turbines, Funazaki and BinSalleh [24] suggested the use of k-ω SST model. Same is true with Zuckerman and Lior [21]. Leon De Paz and Jubran [6,19] presented an extensive evaluation of turbulence model selection for a similar case herein; the results indicated that both the RNG and the SST turbulence models were quite capable of predicting heat transfer and hydrodynamics for impingement in turbine vane. In comparison, it was recommended to use the SST model for its relatively improved prediction. Hence, for the simulation herein, the k-ω SST turbulence model was chosen.

Mesh Sensitivity and Validation

Mesh independence study was conducted by refining the mesh successively until the solution was insensitive. To estimate the discretization error, the absolute error is defined by the difference between the computed solution and exact solution. Since in this case the exact solution is not known, the independent solution is found using Richardson extrapolation theory or grid convergence index (GCI) and later validated [25]. All the refinement methods support mesh refinement procedure for structured hex meshes, where the number of nodes are increased using a refinement factor. This refinement is not supported for hybrid meshes. Hence an effective refinement factor is defined as the ratio of elements in coarse grid to fine grid raised to a fraction of dimensionality of the problem [26] also shown below in equation (4). Refer to reference [26] for equations used to calculate the GCI.

$$r_{effective} = \left(\frac{N_1}{N_2}\right)^{1/D} \tag{4}$$

Where, N_1 and N_2 are the total number of elements for fine and coarser grid respectively. D is the jet diameter. Table 2 illustrates the CGI values and confirms independence. The values shown are for the validation vane used; sensitivity was checked for all tested configurations. In addition, the local heat transfer coefficient values are also provided for last four grids used in Figure 9.

The relative difference in terms of the averaged heat transfer values between the fine and medium was 0.43% and 3.7%, 10.2% for the coarse and extreme coarse grids used respectively. Considering the computational requirements and time required to obtain a solution, the medium grid was used to validate the vane as it closely replicated true solution given the trifling difference in the averaged and local heat transfer values.

Table 2: Mesh Independence Check - GCI Calculation

$r_{effective}$	1.603
GCI Coarse	1.3 %
GCI Fine	0.6 %

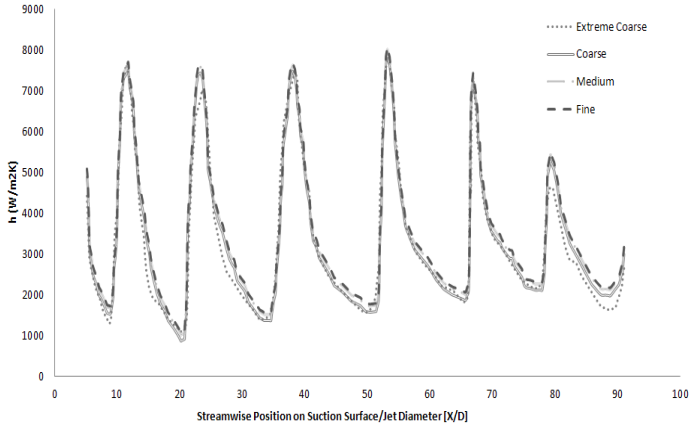

Figure 9: Sensitivity Analysis based on Local Heat Transfer Distribution

Validation of the model was performed against numerical work of Leon De Paz [6][4]. The geometry of the validation vane is depicted in Figure 4 (b). The averaged spanwise pressure at each jet exit is obtained for each row and normalized against plenum pressure. The result is plotted (Figure 10) for jets numbered successively starting at 0 for leading edge and covering the suction and pressure surfaces. The maximum relative error was found to be about 0.09% compared to [6]. Local Nu was also mapped in Figure 11 to assure validity of the vane for further analysis; the abscissa being the curved length of pressure surface non-dimensionalized by the diameter and ordinate the Nu for middle column of jets. The maximum relative error for this case was around 0.8%. With relative errors of less than 1% for key parameters checked, the mesh is considered independent of discretization and mesh errors and valid for further analysis.

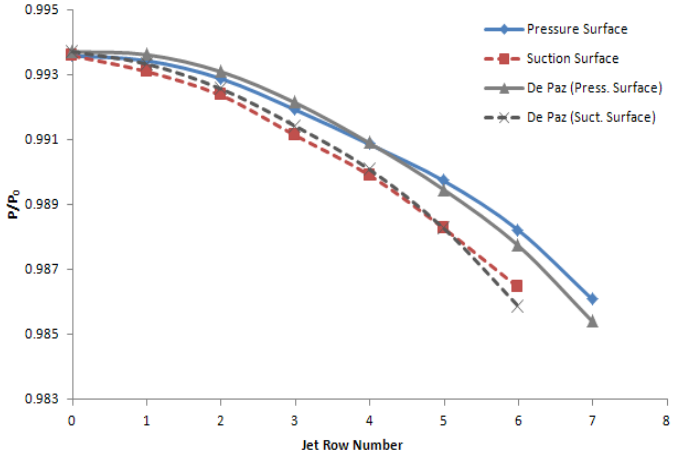

Figure 10: Validation Analysis based on Normalized Pressure at Jet Exit for each Jet Row starting at Leading Edge

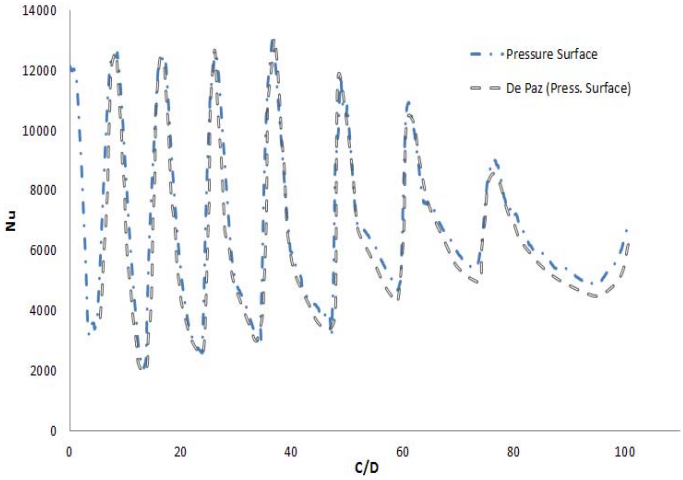

Figure 11: Validation based on Local Nu for Non-Dimensional Curve Length on Pressure Surface along the Mid-plane of Jet Holes.

RESULTS AND DISCUSSION

The effects of changing the inclination and diameter of the nozzles have been considered in the present study. In addition, hydrodynamic effects (effect of pressure, Re distribution, cross-flow and heat transfer) are taken into account and compared accordingly.

Hydrodynamics for Base Vane

The geometry of the base vane is rendered in Figure 4 (c) and initially compared to the validation vane. Flow propagates in the direction of tapering (-Z direction) and the local Nu values is observed to increase compared to the validation vane as perceived from Figure 12. The values computed are on a

[4] Validation for the vane against experimental results (flat plate with corresponding conditions) has been performed. See references [6,19] for more information.

strip lying on the target surface through the middle column of jets[5]. The maximum percent increase in the stagnation value was recorded to be about 10.3% due to the change in airfoil profile. It is interesting to note the change obtained for a span of only 12D.

The effect of streamwise cross-flow becomes prominent starting with the 4th jet; and, as the cross-flow increases moving downstream, the position of the stagnation point shifts away from the jet center location in the direction of cross-flow; this has been marked by vertical lines at the top of Figure 12. Similar cross-flow effects were obtained by numerical work of Leon De Paz [6] and experimental work of Gao [27]. For jet rows 1 through 4, the local heat transfer tends to perform well, increasing marginally. It was realized that the streamwise cross-flow velocity here was less than 10% of the jet average velocity. Such enhancement was seen experimentally by Gao [27] where surface heat transfer was enhanced by low cross-flow velocities. Examination of cross-flow interactions and its influence on heat transfer was performed by Wang et al. [28]. using a 3-D transient liquid crystal scheme. In general it was seen that the jet momentum and the cross-flow buffering effect are in constant competition. When the jet momentum is higher, the jet flow penetrates and local heat transfer values are high. When the cross-flow momentum is higher than the jet flow, a horizontally stretched pattern (almost uniform) of heat transfer is seen.

In comparison of the two models shown in Figure 12, the slope of the drop in stagnation values due to cross-flow was found to be the same (shown in orange and green lines; approximately -100.5) with the vertical distance between them providing the increase in Nu and horizontal distance the shift in stagnation value (~2.75D). The region in between the jets illustrates the effects of forced convection with the least increase in heat transfer due to accelerating exiting flow. Nu contours also explain the above phenomena. Careful examination of Figure 13 (a) reveals the qualitative determination of cross-flow effect. For a single jet, the shape of Nu distribution remains uniform in all directions [2]; however in array of jets the shape changes based on location. The center jet in the figure below is subject to cross-flow from the edge jets and vice versa; also, the jets are subject to spent air from upstream direction. The simplistic sketch (Figure 13 (b)) explains the effect of cross-flow from upstream and edge jets on Nu. In other words, the Nu contour shape expresses the local flow direction. In Figure 13 (a), the plenum flow is in the -Z direction. The impingement flow is moving into the paper where the stagnation zone is seen in red as the jet impinges on the airfoil surface. The arrows show the direction of the streamwise crossflow buildup due to the upstream jets. The influence of cross-flow for multiple jets on heat transfer was experimentally studied by Bouchez and Goldstein [29]. Flow visualization results showed that the interaction between the cross-flow (streamwise and spanwise) and impinging jets made the flow highly three-dimensional, which increased the complexity of the flow structure and the heat transfer distribution. Heat transfer coefficients in general were seen to reduce due to these complex flow interactions. Further investigation of cross-flow effect performed by Wang et al. [28] showed that the heat transfer distribution is highly non-uniform due to the complex 3-D flow structure.

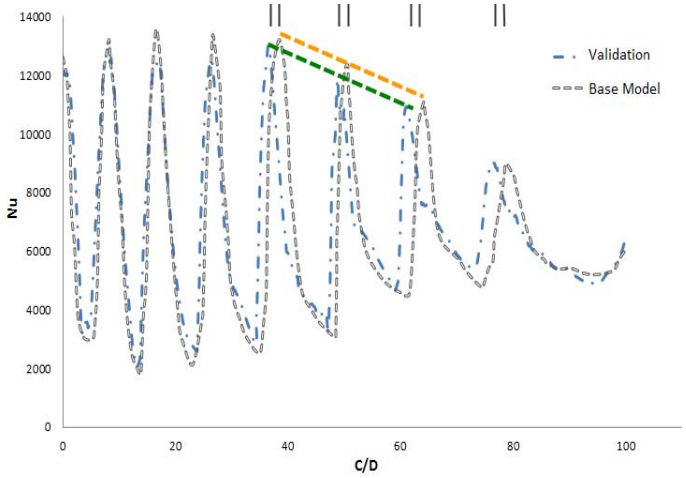

Figure 12: Local Nu Distribution for Validation Vane and Base Vane on Pressure Surface

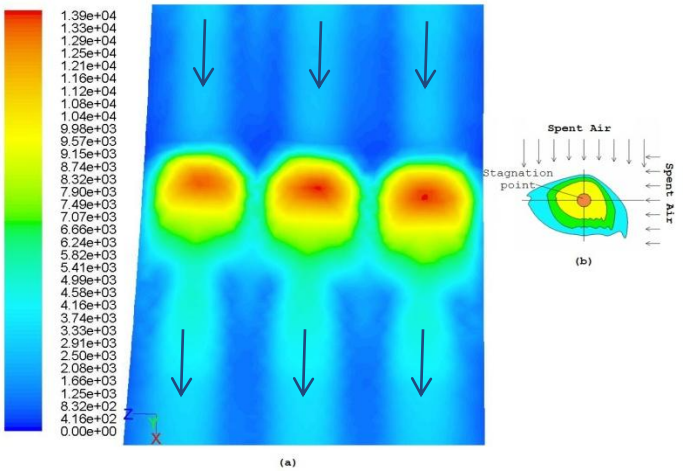

Figure 13: Nu Contours for Jet with Cross-flow (a) Base Vane (b) Simplistic Sketch [27]

The increase in Nu may be related to the increase in the velocity at jet exit location for the two cases shown in Figure 12; the exit velocity is shown on a cutting plane through the 6th row of jet on the pressure surface (see Figure 14). Clearly, the increase in jet velocity is depicted in going from Figure 14 (a) to Figure 14 (b). The average velocity at exit for jet row 6 on pressure surface, middle column, of validation vane was 46.93

[5] For the base model, the L_C is located at the same span where the strip is positioned; L_C is the same for the validation vane. This was done for comparison purposes.

m/s whereas the average for base model was 52.3 m/s. In terms of the change obtained from column 1 to 3, the validation model does not represent any noticeable change in velocity. On the other hand, for the base model, the exit velocity increases in the -Z direction, also showing increased effective heat transfer in Figure 13 (a). The average exit velocities from left to right in Figure 14 (b) are 47.2 m/s, 52.3 m/s and 59.1 m/s.

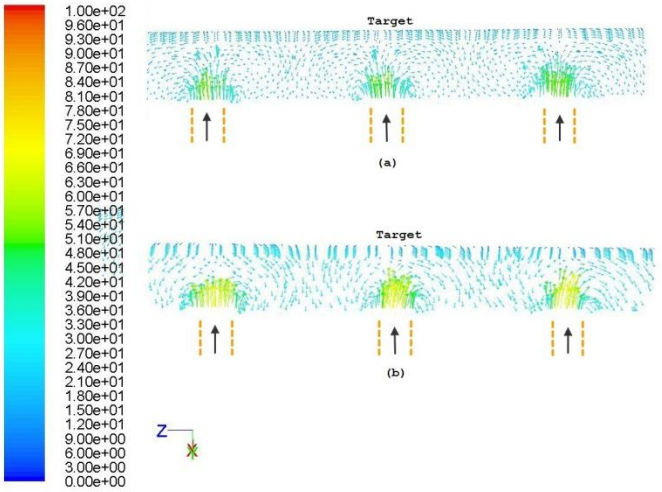

Figure 14: Jet Exit Velocity Vectors [m/s]. Flow is in –Z direction in the plenum. Column 1 jet is the 1st jet (extreme left). (a) Validation Model (b) Base Model

The pressure distribution across the array is of great interest as it affects the exit velocity of the jets, the cross-flow, and therefore, the heat transfer coefficient at each jet row. The absolute pressure is highest in the plenum chamber as represented in Figure 15; using the ideal gas law with equations (1) and (2), allows the micro jets to behave with no slip condition. In the impingement chamber the pressure decreases in the streamwise direction. Thus, the lowest pressure point is found at the trailing edge of the vane. The decrease in pressure can be attributed to the increase in the streamwise crossflow velocity [6]. Using Figure 10 as a reference, the overall pressure drop across the suction surface jets and pressure surface jets are relatively the same. The suction surface and pressure surface curves do not overlap in the figure because of the difference in the number of jets on these surfaces. If pressure values are compared at the same curve length (as opposed to jet row number), the absolute pressure on the pressure surface is higher than that on the suction surface. And, the lower pressure at a given curve length on the suction surface yields higher streamwise cross-flow momentum compared to the pressure surface. The lower absolute pressure on the suction surface and the lowering of pressure along the streamwise direction favors the cross-flow momentum due to the increased mass (from upstream spent air) when compared to the jet flow momentum. Since the cross-flow momentum overpowers the jet flow momentum in the streamwise direction, the cross-flow impedes the performance of the impinging jet by reducing the exit Re. Since the suction surface observed lower pressure, it implies the cross flow momentum shall be higher on the suction surface and hence the impinging jet exit Re shall be degraded for the suction surface when compared to the pressure surface. This is checked using the Re distribution for the jet row numbers graphed in Figure 16. Comparing jet 7 and 5 (they are almost at the same curve length from leading edge) from the pressure surface and suction surface respectively, higher Re is achieved at the pressure surface compared to suction surface.

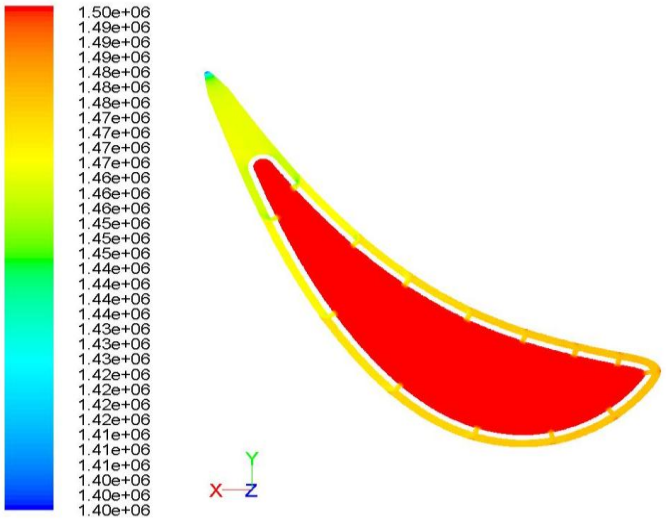

Figure 15: Pressure Contours [Pa] for Base Vane

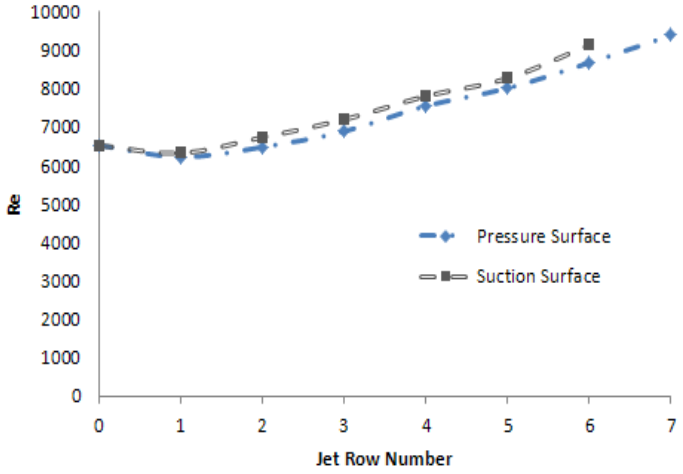

Figure 16: Reynolds Number Distribution at Jet Exit

Effect of Inclination

Heat transfer distributions for impinging array of inclined jets are studied. Figure 5 shows jet configurations used. Jet holes are still 0.51 mm and the effect of inclination is compared to the base vane. The jets are aligned such that the target impingement co-ordinate remains the same to the base model. The flow pattern followed is: flow enters spanwise into the plenum chamber, enters the impingement hole inclined such

that they are in the direction of streamwise cross-flow buildup (+45°) or oppose it (-45°) from the leading edge. The local Nu is plotted in Figure 17.

Examining +45° inclination, the stagnation values drop drastically providing reduced heat transfer at stagnation; this is due to the enhanced effects of cross-flow as the flow is directed in the same route. Similar analysis was performed by Huang et al [7] where the jets were inclined in the same direction; however, the incoming flow was in the streamwise direction as opposed to spanwise direction. Results obtained indicated that the inclined jets had less heat transfer coefficient than straight jets. As mentioned earlier, the cross-flow effects are not apparent in the first few jets where the exit velocity is greater than 10% of the cross-flow velocity. The deviation of the stagnation point due to enhanced cross-flow is observed in the same figure marked by red vertical lines at the top. It is interesting to note that the effect of inclining the jet in the direction of streamwise cross-flow enhances the deviation of stagnation point from the base model; the deviations obtained are 2.5D, 3.95D and 6.25D. That is, the trend followed is similar to $(2.5)^1$, $(2.5)^{1.5}$ and $(2.5)^2$; where 2.5 is the coefficient of the first deviation. Enhancing cross-flow would mean enhancing the convective effects; this can be observed by viewing the slope of the Nu distribution curve. The slope instead of being steep like in the case of the base model is now comparatively gentle. This results in the base of the fountain shaped distribution being wider as seen around the last three jets in Figure 17. The effect can be compared to the velocities shown in Figure 18 (a); where the cross-flow seems to diffuse the impinging jet and hence the reduced Nu effect.

Probing the effects of -45° inclination, using Figure 17, the stagnation Nu value seems to drop from the base model, however the magnitude of the drop is less compared to the +45° case. It is noteworthy to watch the Nu distribution being characterized by a secondary maximum, whose value increases as the flow moves downstream; this is signified by the arrow indicator in the figure. This secondary maximum may be associated with the increase in turbulence level and heavy mixing. That is, the high momentum flow from the jets coupled with velocity fluctuations could be the cause of secondary peaks. This phenomenon may also be contributed by the boundary layers in this region being thin and highly turbulent as in the case of single impingement jets with H/D < 5 [30]. The deviation in the location of stagnation for this case due to streamwise cross-flow is marginal compared to the +45° case. Velocity distribution in Figure 18 (b) shows the variation of velocity magnitude upstream of the jet, at the jet impingement and further downstream of the jet. This fluctuating velocity and heavy mixing with strong eddies are the cause for secondary peaks. This was also seen in the experimental results of Bouchez and Goldstein [29] where the interaction of adjacent jets, streamwise cross-flow build-up and confinement were held responsible for eddying of flow and boundary layer separation just before impingement. Also, such interactions resulted in the formation of secondary heat transfer peaks between jets. The averaged Nu values over the entire target surface showed 11.3% increase for the latter case and 8.9% dip compared to the base vane.

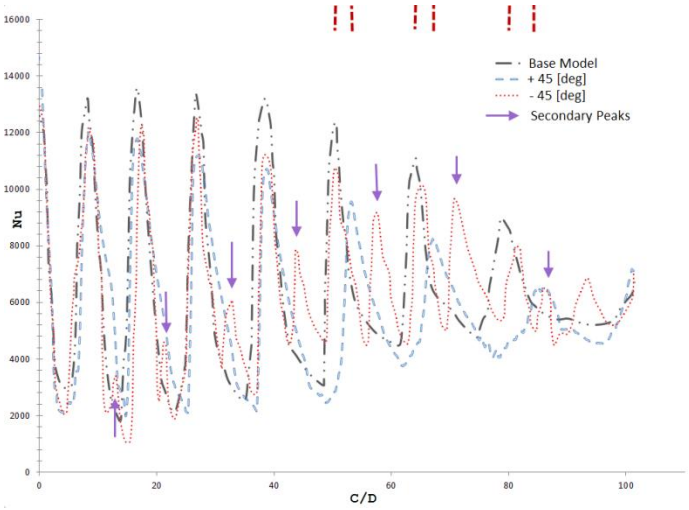

Figure 17: Nu Distribution showing the effects of Impingement Jet Angle on Pressure Surface

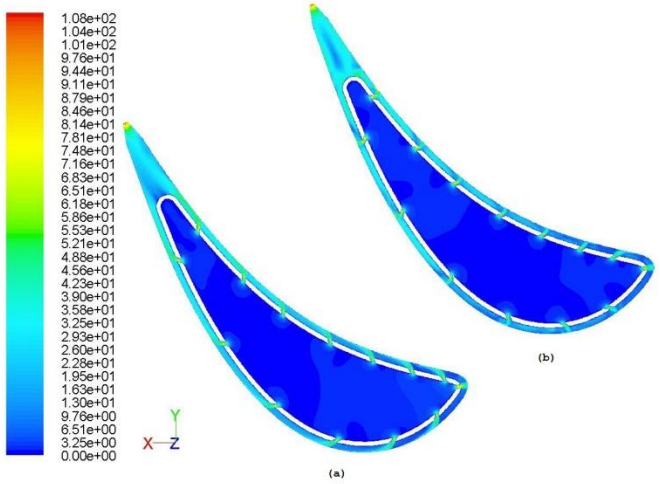

Figure 18: Velocity Distribution for (a) +45° and (b) -45°

Effect of Jet Diameter

The analysis hereunder pertains to the application of micro jet impingement cooling for gas turbine vanes. Hence, to understand the effect of reducing the nozzle diameter to a micro scale of 0.25 mm, and 0.125 mm, the following assumption is made: this model is a simple reduction in jet diameter from the default values. To wit, it is the resultant model where the turbine vane's plenum is assumed to be drilled with an aperture of 0.25 mm and 0.125 mm in lieu of 0.5 mm. It is apparent from Figure 19 that when the diameter of the nozzle is reduced to micro scale, significant improvement in heat transfer coefficient is obtained. In fact, the percent improvement is about 1.5 times, as the diameter is reduced to half. Similar

results have been comprehended by experimental results; for instance, about 20% to 70% increase was seen in stagnation values when the jet diameter was reduced from 1.5 mm to 1 mm in an experimental setup for single jet impingement by Glynn and Murray [12].

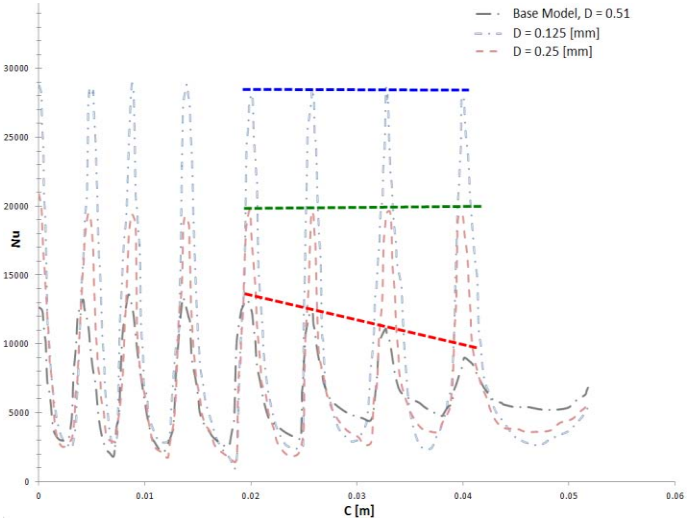

Figure 19: Effect of Jet Diameter

A dimensional curved length was used on the abscissa since the non-dimensional form C/D relies on the diameter which varies across the models. Improvement on the heat transfer is seen for the same mass flow at the inlet of the plenum. It is interesting to note that the effectiveness of the jet impingement is increased compared to base model due to reduced streamwise cross-flow effects. Therefore, there are multiple benefits of micro-jets: they reduce the cross-flow by increasing the spanwise spacing; higher exit Re increase the penetration of the jet and reduced cooling flow lessens the effect of cross-flow; consequentially, this yields a more uniform heat transfer distribution on the airfoil surface. The effect of reduced cross-flow can be noticed by the relatively zero slope of the line joining the stagnation points for D = 0.25 and 0.125 mm shown in green and blue hashed lines as compared to 0.51 mm shown in red. The downside however, apart from plugging, may be the high heat transfer gradient obtained; this may add to the thermal stress map and high thermal loading may shorten the lifespan of the vane [18]. Another shortcoming to reducing the diameter is the demand for higher pressure head. The impingement holes in the vane's plenum can be perceived as an orifice plate. When fluid reaches the orifice, it is forced to converge to go through the small hole. The point of maximum convergence actually occurs downstream of the physical orifice (known as vena contracta). The static pressure at the vena contracta increases as the diameter decreases. To meet this requirement, the flow area in the flow passage decreases, thereby increasing blockage as diameter is reduced [31]. The average Nu however for 0.125 mm surged to about 55% higher than 0.51 mm. The exit Re almost doubled at jet exit as at constant mass flux, reducing the diameter of the nozzle by half, doubles the average Re across the array. This effectively increases the heat transfer obtained. Results for effect of change in Re are known (see references [6,11,12,32] for more information). The streamwise distribution of Re however remains the same.

CONCLUSIONS

Three-dimensional actual shaped turbine vane geometry of the NASA GE E^3 engine was numerically studied for the effects of change in diameter and inclination of 42 micro jets. The diameters investigated include 0.51 mm, 0.25 mm and 0.125 mm. The inclinations altered were +45° and -45°. For simplicity, validation and better understanding the nature of impingement heat transfer, the airfoil surfaces were provided with a constant temperature boundary condition. Moreover, it was assumed that the flow in its entirety exits from the trailing edge and no leakages occur (especially at inter-stage seal); also, the vane considered did not support film cooling. Validation was performed against existing numerical results on a simplified model with no spanwise tapering or twisting.

Results for airfoil with tapering and twisting yielded better heat transfer results as the flow moved in the tapered span direction. Cross-flow was seen to impede the effective impingement heat transfer distribution. The effects however were not prominent for the first few jet rows, where it was witnessed that if the average exit velocity was greater than the spend air velocity, the heat transfer distribution was improved or remained almost the same.

The results obtained for reduction in nozzle diameter indicate that the Re at the jet exit almost doubles and improves the heat transfer substantially. Another added benefit to reduced diameter is the lessened cross-flow effect. Uniform heat transfer distribution is thus observed for both the cases considered: 0.25 and 0.125 mm jet diameter. On the other hand the small diameter leads to higher effective thermal stresses and may be prone to plugging.

The effects of changing the inclination of nozzles were also studied. Two cases were considered, one where the inclination of the nozzle supported the streamwise cross-flow and the other opposed it. Although both cases did not produce improvement in terms of stagnation values compared to the base model, the inclination of -45° yielded secondary peaks and an overall improvement in the averaged Nu. +45° tilt of nozzle improved the streamwise cross-flow effect and thus the convective heat transfer, but reduced the effectiveness of impingement heat transfer. The deviation in the position of stagnation Nu number increased in the stream wise direction.

NOMENCLATURE

Latin and Abbreviations

C	Curve length
CFD	Computational Fluid Dynamics
d	Diameter of air molecule

D	Nozzle/Jet diameter
E^3	Energy Efficient Engine (developed by GE)
GCI	Grid Convergence Index
h	Convective heat transfer coefficient
H	Nozzle to target (inner airfoil surface) spacing
hex	Hexahedral
k	Thermal conductivity of coolant
K_n	Knudsen number
L	Nozzle length
L_c	Characteristic Length (chord at mid span)
N_1	Total number of elements for fine grid
N_2	Total number of elements for coarse grid
N_A	Avogadro's number
Nu	Nusselt number
P	Absolute pressure
q	Surface heat flux
r	Radial direction
R	Universal Gas Constant
Re	Reynolds number
$r_{effective}$	Effective refinement factor
T	Temperature
-Z	Spanwise direction

Greek and Subscripts

λ	Mean free path
$_s$	Surface
$_j$	Jet

REFERENCES

[1] Halila, E., Lenahan, D. and Thomas, T., 1982, "Energy Efficient Engine: High Pressure Turbine Test Hardware Detailed Design Report," NASA CR-167955, pp. 1-194.

[2] Han, J., Dutta, S. and Ekkad, S., 2000, *Gas Turbine Heat Transfer And Cooling Technology*, Taylor & Francis, pp. 1-25.

[3] Koopman, R. and Sparrow, E., 1976, "Local and Average Heat Transfer Coefficients due to an Impinging Row of Jets," Int. J. Heat and Mass Transfer, 19, pp. 673-683.

[4] Florschuetz, L., Berry, R. and Metzger, D., 1980, "Periodic Streamwise Variations of Heat Transfer Coefficients for Inline and Staggered Arrays of Circular Jets with Cross-flow of Spent Air," ASME J. of Heat Transfer, 102, pp. 132-137.

[5] Martin, H., 1977, "Heat and Mass Transfer between Impinging Gas," 1977, Adv. in Heat Transfer, 13, pp. 1-60.

[6] Leon De Paz, M., 2009, "A Numerical Study of Impinging Jets Inside a Turbine Vane," M.A.Sc.Thesis, Department of Aerospace Engineering, Ryerson University, Toronto.

[7] Huang, Y., Ekkad, S. and Han, J., 1996, "Detailed Heat Transfer Coefficient Distributions Under an Array of Inclined Impinging Jets using a Transient Liquid Crystal Technique," 9th Int. Symp. on Transport Phenomena in Thermal Fluids Eng.

[8] Treuren, V., Wang, Z., Ireland, P. and Jones, T., 1996, "Comparison and Prediction of Local and Average Heat Transfer Coefficients under an Array of Inline and Staggered Impinging Jets," IGTI Congress and Exhibition, Birmingham.

[9] Vantreuren, K., 1994, "Impingement Flow Heat Transfer Measurements of Turbine Blades Using a Jet Array," Ph.D. Thesis, University of Oxford.

[10] Kercher, D. and Tabakoff, W., 1970, "Heat Transfer by a Square Array of Round Air Jets Impinging Perpendicular to a Flat Surface Including the Effect of Spent Air," J. Engineering for Power, 92, pp. 73-82.

[11] Lee, J. and Lee, S., 1998, "Stagnation Region Heat Transfer of a Turbulent Axisymmetric Jet Impingement," Expt. Heat Transfer, 12(2), pp. 137-156.

[12] Glynn, C. and Murray, D., 2005, "Jet Impingement Cooling in Microscale," ECI Int. Conf. on Heat Transfer & Fluid Flow in Microscale, pp. 1-7.

[13] Date, A., 2005, *Introduction to Computational Fluid Dynamics,* Cambridge University Press.

[14] Hadjiconstantinou, N., and Simek, O., 2002, "Constant-Wall-Temperature Nusselt Number in Micro and Nano-Channels," J. of Heat Transfer, 124, pp. 356-364.

[15] Grindle, T., Burcham, F., and Hugh L., 2003, "Engine Damage to a NASA DC-8-72 Airplane from a High-altitude Encounter with a Diffuse Volcanic Ash Cloud," NASA TM-2003-212030, Technical Memorandum.

[16] Hall, K., 1989, Dirt Removal Means for Air Cooled Blades, Patent. no. 4,820,123 USA.

[17] Land, C., Joe, C., and Thole, K., 2010, "Considerations of Double-Wall Cooling Design to Reduce Sand Blockage," Proc. of ASME Turbo Expo 2008: Power for Land, Sea and Air.

[18] Timko, L., 1984, "Energy Efficient Engine: High Pressure Turbine Component Performance Report," NASA CR-168289.

[19] León De Paz, M. and Jubran, B., 2010, "A Numerical Study of an Impingement Array inside a 3-D Turbine Vane," Proc. of ASME Turbo Expo: Power for Land, Sea and Air.

[20] FLUENT INC., 2006, *FLUENT 6.3 User's Guide*.

[21] Zuckerman, N. and Lior, N., 2005, "Impingement Heat Transfer: Correlations and Numerical Modeling," ASME J. Heat Transfer, 127, pp. 544-552.

[22] A-Frost, S. and Jambunathan, K., 1996, "Numerical Prediction of Semi-Confined Jet Impingement and Comparison with Experimental Data," Int. J. Num. Meth. Fluids, 23, pp. 295-306.

[23] Isman, M., Pulat, E. and Etemoglu, A., 2008, "Numerical Investigation of Turbulent Impinging Jet Cooling of a Constant Heat Flux Surface," Numerical Heat Transfer, Part A: Applications, 53(10), pp. 1109-1132.

[24] Funazaki, K. and BinSalleh, H., 2008, "Extensive Studies on Internal and External Heat Transfer Characteristics of Integrated Impingement Cooling Structures for HP Turbines," Proc. of ASME Turbo Expo, Berlin.

[25] Cadafalch, J., Pérez-Segarra, C., and Consul, R., 2002, "Verification of Finite Volume Computations on Steady-State Fluid Flow and Heat Transfer," J. of Fluids Eng., 124(11).

[26] Roache, P., 1994, "Perspective: A Method for Uniform Reporting of Grid Refinement Studies," J. of Fluids Eng., 116, pp. 405-413.
[27] Gao, L., 2003, "Effect of Jet Hole Arrays Arrangement on Impingement Heat Transfer," M.A.Sc Thesis, Louisiana State University, pp. 1-73.
[28] Wang, T., Lin, M., and Bunker, R.S., 2005, "Flow and Heat Transfer of Confined Impingement Jets Cooling using a 3-D Transient Liquid Crystal Scheme," Int. J. Heat and Mass Transfer, 48, pp. 4887-4903
[29] Bouchez, J. –P. and Goldstein, R. J., 1975, "Impingement Cooling from a Circular Jet in a Cross Flow," Int. J. Heat Mass Transfer, 18(6), pp. 719-730.
[30] Incropera, F. and DeWitt D., 2007, *Fundamentals of heat and mass transfer,* John Wiley & Sons, Inc., 6 Ed., pp. 447-452.
[31] Yan, Y. and Thorpe, R.B., 1990, "Flow Regime Transitions Due to Cavitation in the Flow Through an Orfice," Int. J. Multiphase Flow, 16(6), pp. 1023-1045
[32] Gardon, R., and Akfirat, J., 1965, "The Role of Turbulence in Determining the Heat-Transfer Characteristics of Impinging Jets," Int. J. of Heat and Mass Transfer, 8(10), pp. 1261-1272.